Alpha-spallation cross sections at 920 MeV (230 MeV/N) in ^{27}Al, ^{16}O, ^{12}C, and ^{9}Be, and application to cosmic-ray transport*

Jonathan R. Radin†
Tel-Aviv University, Department of Physics & Astronomy, Ramat Aviv, Israel

Alan R. Smith and Nickey Little
Lawrence Berkeley Laboratory, University of California, Berkeley, California 94720

(Received 29 November 1973)

We investigated the effects on cosmic rays from spallation reactions between cosmic rays and interstellar helium. The spallation cross sections were measured by exposing thin-sandwich targets to the 920-MeV (230-MeV/N) external α-particle beam of the 184-in. cyclotron at Lawrence Berkeley Laboratory. Cross sections were measured for the production: from ^{27}Al of ^{18}F (12.5 ± 0.5 mb); from ^{16}O of ^{15}O (46.4 ± 2.7 mb), ^{13}N (6.75 ± 0.5 mb), ^{11}C (18.5 ± 0.9 mb), and ^{7}Be (18.5 ± 1.3 mb); from ^{12}C of ^{7}Be (20.0 ± 1.2 mb); and from ^{9}Be of ^{7}Be (12.6 ± 0.8 mb). We constructed spallation cross-section ratios for the ratio of α-particle-induced to proton-induced reactions ($\equiv \Sigma_p^\alpha$). We parametrized this ratio by the nucleon difference (ΔA) between the target initial and final states and we fitted this ratio [$\Sigma_p^\alpha(\Delta A)$] to a linear function in ΔA. We used this function [$\Sigma_p^\alpha(\Delta A)$] to obtain all of the α-particle–spallation cross sections from the corresponding proton-spallation cross sections for targets and products in the elemental range $3 \leq Z \leq 8$, and we applied these cross sections to a cosmic-ray transport calculation wherein we investigated the sensitivity of the cosmic-ray L/M ratio [=(Li + Be + B) / (C + N + O)] and of the abundances of the L and M elements to the helium fraction of the interstellar gas.

[NUCLEAR REACTIONS ^{27}Al(α,x)^{18}F; ^{16}O(α,x)^{15}O, ^{13}N, ^{11}C, ^{7}Be; ^{12}C(α,x)^{7}Be; ^{9}Be(α,x)^{7}Be, E = 920 MeV; measured σ; NaI detector. Examined effect interstellar He on cosmic rays.]

INTRODUCTION

Basic to the understanding of cosmic-ray propagation is a knowledge of the nuclear spallation cross sections for reactions between cosmic rays and the interstellar gas (85–90% hydrogen and 15–10% helium).[1] Of primary interest are interactions of incident cosmic-ray nuclei from the relatively copius M group (C, N, O) producing final-state nuclei of the L group (Li, Be, B). In the past much effort has been made measuring these spallation reactions with proton beams[2] (taking the place of interstellar hydrogen gas) and recently with α-particle beams[3–6] (taking the place of interstellar helium gas).

We report first on additional measurements of spallation cross sections of the nuclei ^{27}Al, ^{16}O, ^{12}C, and ^{9}Be in interactions with 920-MeV α particles. We use the symbols: E_x for the kinetic energy of the nucleus x; E_x/N for the kinetic energy per nucleon of the nucleus x, where N is the number of nucleons in the nucleus x; Σ_p^α for the generic term for the ratio of the α-particle cross section to the p cross section; $\Sigma_p^\alpha(A, B)$ for the ratio of the cross sections for the inclusive isotopic-production processes $[A(\alpha, x)B]/[A(p, x)B]$, where A and B are the initial- and final-state nuclei, respectively, and where x is any remaining particle(s); $\Sigma_p^\alpha(\Delta A)$ for the functional dependence of Σ_p^α on ΔA, where ΔA is the nucleon difference between the target initial and final states; $\Lambda(L/M = 0.25)$ for the mass of interstellar gas traversed to produce a cosmic-ray L/M ratio [=(Li + Be + B)/(C + N + O)] of 0.25.[7,8] Secondly, we report: making simple assumptions for $\Sigma_p^\alpha(\Delta A)$ and for the cosmic-ray composition, we transport the cosmic rays through the interstellar gas developing the cosmic-ray L/M ratio; we examine the sensitivity of the quantity $\Lambda(L/M = 0.25)$ and of the elemental abundances of the constituent members of the L group and M group (at $L/M = 0.25$ [7,8]) to the He/(H + He) ratio of the interstellar gas. The transport model chosen is the one-dimensional slab approximation wherein all species traverse an equal amount of matter.

EXPERIMENTAL PROCEDURES

Targets consisting of 3.81-cm-diam thin sandwiches (Fig. 1) were exposed to the external 920-MeV (230-MeV/N) α-particle beam in the medical cave of the 184-in. cyclotron at Lawrence Berkeley Laboratory (LBL). The beam was focused to a diameter of $\approx$2.5 cm on which the targets were centered. The neutron and deuteron contaminations of the beam had been studied previously and

were negligible.[3] The targets were counted in the low-background cave of the Health Physics Group at LBL. The ^{16}O target was BeO and, as the Be (100% ^{9}Be) present contributed to the ^{7}Be production, we separately measured $\sigma[^{9}Be(\alpha, x)^{7}Be]$ with Be targets and subtracted its contribution to the ^{7}Be production in BeO. In Table I the pertinent information of the isotopes examined is tabulated.[9]

Targets

All targets (Fig. 1) were sandwiches (3.81-cm diam) consisting of two or three subtargets [main and monitor(s)]. Each subtarget consisted of guard foils or disks and the central counted disk. The constituents were:

^{12}C. Polystyrene $(CH)_n$ disks 0.16 cm (0.17 g/cm^2) thick with 0.008-cm polyethylene guard foils. The carbon cross sections are based on the total carbon ($^{12}C+^{13}C$) content.

BeO. Ceramic disks 0.075 cm (0.26 g/cm^2) and 0.32 cm (0.95 g/cm^2) thick and 99.5% pure. The front and rear guard disks were 0.075 and 0.32-cm BeO disks, respectively. The contamination was determined by spectrometric analysis to be $(1.0^{+1.0}_{-0.5})$% Mg plus trace quantities of other elements. The oxygen was taken to be 100% ^{16}O.

Be. A vacuum-deposited Be disk (impurity 60 ppm) 0.075 cm (0.13 g/cm^2) thick. The front and rear guard disks were 0.02 and 0.32-cm Be. No radiation other than ^{7}Be was observed.

Al. 99.99% Al foils of thickness 0.008 cm (0.23 g/cm^2) for monitoring and 0.013 cm (0.035 g/cm^2) for $\sigma[^{27}Al(\alpha, x)^{18}F]$ determinations. The guard foils were 0.004 cm thick.

Beam monitors

The beam monitors for all cross-section determinations were radioisotopes produced in the target disks. For short (not ^{7}Be) half-lives the $^{12}C(\alpha, x)^{11}C$ reaction with a cross section of 48.9 $\pm$ 1.8 mb[3] was used. For ^{7}Be production runs, exposure times of 2–10 min required a longer half-life monitor and the $^{27}Al(\alpha, x)^{18}F$ reaction was used. This cross section we separately determined relative to the $^{12}C(\alpha, x)^{11}C$ reaction as $\sigma[^{27}Al(\alpha, x)^{18}F] = 12.5 \pm 0.5$ mb. The final ^{7}Be production cross section in ^{12}C was the average of the results from the ^{11}C and ^{18}F monitor reactions. In addition, as there were many $^{12}C(\alpha, x)^{7}Be$ runs (with all but one run in good agreement) the $^{12}C(\alpha, x)^{7}Be$ reaction in the polystyrene (with a cross section of 20.0 $\pm$ 1.1 mb) was used as an additional monitor for the ^{7}Be production cross-section measurements in BeO and Be. The final ^{7}Be production cross sections in BeO and Be were the average of the results from the three monitor reactions.

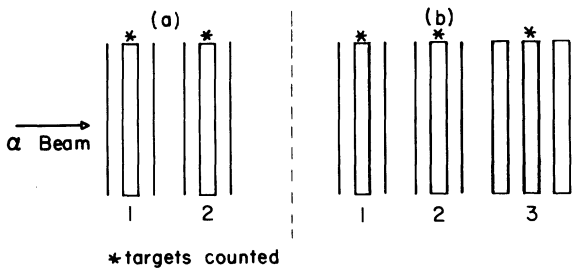

FIG. 1. Target arrangements. α-particle beam incident from the left. Target subsets (1, 2, and 3) consist of two guard foils and a central, counted disk (see text). Set (a): for $^{27}Al \rightarrow {}^{18}F$ and for $^{12}C \rightarrow {}^{7}Be$; 1, Al; 2, $(CH)_n$. For $^{16}O \rightarrow$ (^{15}O, ^{13}N, ^{11}C); 1, $(CH)_n$: 2, BeO. Set (b): for $^{12}C \rightarrow {}^{7}Be$ and $BeO \rightarrow {}^{7}Be$; 1, $(CH)_n$; 2, Al; 3, BeO; for $^{12}C \rightarrow {}^{7}Be$ and $^{9}Be \rightarrow {}^{7}Be$; 1, $(CH)_n$; 2, Al: 3, Be.

Counting apparatus

The detection system consisted of a 20.4-cm-diam $\times$ 10.2-cm-thick NaI(Tl) crystal optically coupled with Dow-Corning DC200 silicone grease to a 12.7-cm-diam EMI 9530-Q photomultiplier (face plate and part of the envelope are fused quartz). The system is housed inside 10.2 cm of low-activity lead bricks. A more complete description is found in Ref. 10. After exposure, the β^+ decaying targets were placed between Cu plates sufficiently thick to stop the β^+; the γ decaying targets were placed directly on the cover plate of the NaI crystal. The output of the photomultiplier was preamplified, double-delay line shaped, and then pulse-height analyzed by a gain-stablized 1600-channel Victoreen (SCIPP 1600) analyzer. For β^+ accumulation, the gain was stabilized on the 511-keV peak and for ^{7}Be counting on the 478-keV peak. In all cases the counting interval was 380–610 keV. The dead time was extensively analyzed[4] and to minimize dead-time corrections, no counts were used in the fittings when count rates were $>150 \times 10^3$/min, except for one $^{16}O \rightarrow {}^{15}O$ run. The largest corrections for dead-time effects were for $^{16}O \rightarrow {}^{15}O$, which re-

TABLE I. Decay features of radioisotopes produced (see Ref. 9).

	Isotope				
	^{18}F	^{15}O	^{13}N	^{11}C	^{7}Be
Half-life (min)	109.7	2.05	9.96	20.35	77180 (53.6 days)
Decay	β^+	β^+	β^+	β^+	478-keV γ
Branching ratio	0.97	1.00	1.00	0.998 (taken as 1.00)	0.103

sulted in 3% changes in the initial quantities of ^{15}O produced by the fitting algorithm.

Runs and fittings

There were two runs to determine the $\sigma[^{27}Al(\alpha,x)^{18}F]/\sigma[^{12}C(\alpha,x)^{11}C]$ ratio and the resultant cross section [Fig. 1(a)]. Initial counts were recorded in 1-min intervals and the target was counted for several days. The β^+ peak was least squares fitted to half-lives of 2.05 min (^{15}O), 9.96 min (^{13}N), 20.35 min (^{11}C), 109.7 min (^{18}F), and 894 min (^{24}Na); the background was both free and fixed (a 10-min ^{27}Mg component was observed but not analyzed). The fitted ^{18}F quantity was found insensitive (<1% initial quantity changes) to variations at the ends of the fitting routine: (1) at the short half-life end by varying the time between the end of exposure and the start of the fitting

TABLE II. Targets, exposure times, and ratios of cross section to monitor cross section.

Target	Weight (g)	Length of exposure (sec)	Count rate (± error %) [a]	Reaction (monitor reaction)	Ratio to monitor (± random error %)	Reaction (monitor reaction)	Ratio to monitor (± random error %)	Reaction (monitor reaction)	Ratio to monitor (± random error %)
Al	0.3968	120	1.15×10^6 (1)	$^{27}Al \rightarrow {}^{18}F$ ($^{12}C \rightarrow {}^{11}C$)	0.252 (1.6)				
Al	0.3455	60	1.57×10^6 (1)	$^{27}Al \rightarrow {}^{18}F$ ($^{12}C \rightarrow {}^{11}C$)	0.258 (1.6)				
Systematic errors in the above ratios					0.0%				
BeO	2.983	6	2.04×10^6	$^{16}O \rightarrow {}^{15}O$ ($^{12}C \rightarrow {}^{11}C$)	0.957 (2.3)	$^{16}O \rightarrow {}^{13}N$ ($^{12}C \rightarrow {}^{11}C$)	0.135 (6.4)	$^{16}O \rightarrow {}^{11}C$ ($^{12}C \rightarrow {}^{11}C$)	0.381 (2.2)
BeO	2.897	4	0.106×10^6	$^{16}O \rightarrow {}^{15}O$ ($^{12}C \rightarrow {}^{11}C$)	0.950 (1.8)	$^{16}O \rightarrow {}^{13}N$ ($^{12}C \rightarrow {}^{11}C$)	0.141 (6.6)	$^{16}O \rightarrow {}^{11}C$ ($^{12}C \rightarrow {}^{11}C$)	0.377 (3.1)
BeO [b]	2.897	4	0.763×10^6	$^{16}O \rightarrow {}^{15}O$ ($^{12}C \rightarrow {}^{11}C$)	0.680 (1.8)	$^{16}O \rightarrow {}^{13}N$ ($^{12}C \rightarrow {}^{11}C$)	0.125 (5.8)	$^{16}O \rightarrow {}^{11}C$ ($^{12}C \rightarrow {}^{11}C$)	0.370 (2.0)
Systematic errors in the above ratios					1.0%		1.0%		1.0%
$(CH)_n$	1.907	60	20.5 (4)	$^{12}C \rightarrow {}^{7}Be$ ($^{12}C \rightarrow {}^{11}C$)	0.397 (6.3)	$^{12}C \rightarrow {}^{7}Be$ ($^{27}Al \rightarrow {}^{18}F$)	1.58 (6.3)		
$(CH)_n$	1.705	120	35.8 (1)	$^{12}C \rightarrow {}^{7}Be$ ($^{12}C \rightarrow {}^{11}C$)	0.403 (7.5)	$^{12}C \rightarrow {}^{7}Be$ ($^{12}Al \rightarrow {}^{18}F$)	1.54 (3.7)		
$(CH)_n$	1.843	600	197 (1)	$^{12}C \rightarrow {}^{7}Be$ ($^{12}C \rightarrow {}^{11}C$)	0.413 (1.8)	$^{12}C \rightarrow {}^{7}Be$ ($^{27}Al \rightarrow {}^{18}F$)	1.59 (1.8)		
$(CH)_n$ [c]	1.975	300	134	$^{12}C \rightarrow {}^{7}Be$ ($^{12}C \rightarrow {}^{11}C$)	0.354	$^{12}C \rightarrow {}^{7}Be$ ($^{27}Al \rightarrow {}^{18}F$)	1.60		
$(CH)_n$	1.950	600	200 (2)	$^{12}C \rightarrow {}^{7}Be$ ($^{12}C \rightarrow {}^{11}C$)	0.413 (2.5)	$^{12}C \rightarrow {}^{7}Be$ ($^{27}Al \rightarrow {}^{18}F$)	1.62 (2.5)		
$(CH)_n$	1.916	600	189 (2)	$^{12}C \rightarrow {}^{7}Be$ ($^{12}C \rightarrow {}^{11}C$)	0.416 (2.5)	$^{12}C \rightarrow {}^{7}Be$ ($^{27}Al \rightarrow {}^{18}F$)	1.57 (2.5)		
Systematic errors in the above ratios					2.0%		2.0%		
BeO	2.991	600	245 (2)	$BeO \rightarrow {}^{7}Be$ ($^{12}C \rightarrow {}^{11}C$)	0.631 (2.4)	$BeO \rightarrow {}^{7}Be$ ($^{27}Al \rightarrow {}^{18}F$)	2.61 (2.5)	$BeO \rightarrow {}^{7}Be$ ($^{12}C \rightarrow {}^{7}Be$)	1.528 (3.1)
BeO	10.82	120	181 (2)	$BeO \rightarrow {}^{7}Be$ ($^{12}C \rightarrow {}^{11}C$)	0.623 (7.3)	$BeO \rightarrow {}^{7}Be$ ($^{27}Al \rightarrow {}^{18}F$)	2.48 (3.2)	$BeO \rightarrow {}^{7}Be$ ($^{12}C \rightarrow {}^{7}Be$)	1.538 (3.8)
Systematic errors in the above ratios					2.4%		2.4%		1.0%
Be	1.474	600	133 (2)	$^{9}Be \rightarrow {}^{7}Be$ ($^{12}C \rightarrow {}^{11}C$)	0.263 (2.4)	$^{9}Be \rightarrow {}^{7}Be$ ($^{27}Al \rightarrow {}^{18}F$)	1.016 (2.4)	$^{9}Be \rightarrow {}^{7}Be$ ($^{12}C \rightarrow {}^{7}Be$)	0.628 (3.0)
Be	1.474	600	144 [d] (2)	$^{9}Be \rightarrow {}^{7}Be$ ($^{12}C \rightarrow {}^{11}C$)	0.261 (3.2)	$^{9}Be \rightarrow {}^{7}Be$ ($^{27}Al \rightarrow {}^{18}F$)	0.992 (3.2)	$^{9}Be \rightarrow {}^{7}Be$ ($^{12}C \rightarrow {}^{7}Be$)	0.628 (3.3)
Systematic errors in the above ratios					2.2%		2.2%		0.0%

[a] Count rate above background, at end of exposure, of isotopes in the adjacent column, in counts per min. See text for errors in ^{15}O, ^{13}N, and ^{11}C production in BeO.

[b] Run discarded because of large deviation.

[c] Run discarded because of large χ^2 in the fit.

[d] Count rate above residual count rate from previous exposure.

routine, and by inclusion of a 1-min half-life in the fit; and (2) at the long half-life end by varying the time between the end of exposure and the end of the fitting routine, and by letting background be both fitted and fixed (fitted and observed background agreed to within 5%). The initial quantity of ^{18}F was determined relative to the ^{11}C in the monitor to within 2%.

There were six runs to determine the two ratios $\sigma[^{12}C(\alpha,x)^{7}Be]/\sigma[^{27}Al(\alpha,x)^{18}F]$ and $\sigma[^{12}C(\alpha,x)^{7}Be]/\sigma[^{12}C(\alpha,x)^{11}C]$ and the subsequent $^{12}C(\alpha,x)^{7}Be$ cross section. One run produced a large χ^2 in the fit and was not included in the final averaging.

There were two runs to measure the three ratios of $\sigma[^{9}Be(\alpha,x)^{7}Be]$ to the three monitor cross sections $\sigma[^{12}C(\alpha,x)^{11}C]$, $\sigma[^{27}Al(\alpha,x)^{18}F]$, and $\sigma[^{12}C(\alpha,x)^{7}Be]$, and the subsequent $^{9}Be(\alpha,x)^{7}Be$ cross section. Both monitor disks were incorporated together with the Be disk into one target package and irradiated together [Fig. 1(b)]. The Be target was reused and the residual ^{7}Be in the second exposure was carefully measured and was (32.5 ± 0.5)% of the ^{7}Be produced in the second exposure. Both runs agreed to within 1%.

There were three runs to measure the three ratios of $\sigma[^{16}O(\alpha,x)^{15}O]$, $\sigma[^{16}O(\alpha,x)^{13}N]$, and $\sigma[^{16}O(\alpha,x)^{11}C]$ relative to the monitor reaction $\sigma[^{12}C(\alpha,x)^{11}C]$ [Fig. 1(a)]. The third run for ^{15}O production, reusing the previous target, inexplicably gave a small cross section, much in disagreement with the other two runs, and was not included in the final averages. The radioactive-decay counts were accumulated at 1-min intervals and least squares fitted to 2.05-, 9.96-, and 20.35-min half-lives. The variations in the fitting routine discussed for the $^{27}Al(\alpha,x)^{18}F$ runs were repeated here, except for not including a fit to a 1-min half-life component. This procedure resulted in uncertainties in each of the three exposures of 2, 2, and 2% for ^{15}O and ^{11}C; and 3, 6, and 6% for ^{13}N.

There were two runs to measure the three ratios of $\sigma[BeO(\alpha,x)^{7}Be]$ to the three monitor cross sections $\sigma[^{12}C(\alpha,x)^{11}C]$, $\sigma[^{27}Al(\alpha,x)^{18}F]$, and $\sigma[^{12}C(\alpha,x)^{7}Be]$ [Fig. 1(b)]. The three ratios of $\sigma[^{16}O(\alpha,x)^{7}Be]$ to the three monitor cross sections were each determined by subtracting the ratio of $\sigma[^{9}Be(\alpha,x)^{7}Be]/\sigma$(monitor reaction) from the ratio of $\sigma[BeO(\alpha,x)^{7}Be]/\sigma$(monitor reaction) for the corresponding monitor reaction.

Of the six runs for ^{7}Be production in ^{12}C, (a) one run was independent and the remaining runs were the same as those used for (b) one measurement of the cross-section ratio $\sigma[^{27}Al(\alpha,x)^{18}F]/\sigma[^{12}C(\alpha,x)^{11}C]$ and (c) two measurements of ^{7}Be production in BeO and (d) two measurements of ^{7}Be in ^{9}Be. All of the final ^{7}Be production cross sections were the average of the results from each of the three monitors, and as these measurements were dependent, the final error was the average error. In Tables II and III are tabulated the quantities of interest regarding the ratios of (cross section)/σ(monitor reaction) and the resultant cross sections.

Uncertainties

The photoabsorption efficiency of NaI(Tl) for the 478-keV γ ray of ^{7}Be was taken to be the same as for the 511-keV annihilation γ ray within a systematic error of 1%. The 478-keV γ efficiency of the entire NaI system (including effects of multiple scattering inside the detector housing and the use of different target-holder assemblies for ^{7}Be and ^{11}C targets) differed from the β^+ efficiency in two ways. First, the spectrum of the β^+ counts showed, in addition to the primary peak at 511 keV, a second peak at 710 keV which was interpreted as the sum peak of one annihilation γ ray plus the backscattered second γ ray and thus, represented β^+ counts lost relative to ^{7}Be counts. The energy sum of a 511-keV and 180° backscattered 511-keV γ ray is 767 keV, consistent with the peak location. The area of the sum peak was (5.7 ± 0.2)% of the area of the main peak. Second, the Cu plates placed around the β^+ decaying targets but not around the

TABLE III. Ratios of cross sections to monitor cross sections and cross-section values. The cross section for $BeO(\alpha,x)^{7}Be$ is included for convenience. The cross sections are based on $\sigma[^{12}C(\alpha,\alpha n)^{11}C]$ of 48.9 ± 1.8 mb (Ref. 3).

Reaction	Monitor reaction	Ratio to monitor (±%)	Cross section (mb) (±%)
$^{27}Al \rightarrow {}^{18}F$	$^{12}C \rightarrow {}^{11}C$	0.255 ± 1.8	12.5 ±4
$^{16}O \rightarrow {}^{15}O$	$^{12}C \rightarrow {}^{11}C$	0.953 ± 3	46.6 ±6
$^{16}O \rightarrow {}^{13}N$	$^{12}C \rightarrow {}^{11}C$	0.138 ± 6	6.75 ± 7
$^{16}O \rightarrow {}^{11}C$	$^{12}C \rightarrow {}^{11}C$	0.380 ± 3	18.5 ±5
$^{12}C \rightarrow {}^{7}Be$	$^{12}C \rightarrow {}^{11}C$	0.413 ± 3	20.2 ±6
$^{12}C \rightarrow {}^{7}Be$	$^{27}Al \rightarrow {}^{18}F$	1.59 ±3	19.9 ±6
$^{12}C \rightarrow {}^{7}Be$	Average		20.0 ±6
$BeO \rightarrow {}^{7}Be$	$^{12}C \rightarrow {}^{11}C$	0.631 ± 5	30.8 ±6
$BeO \rightarrow {}^{7}Be$	$^{27}Al \rightarrow {}^{18}F$	2.56 ±5	32.0 ±6
$BeO \rightarrow {}^{7}Be$	$^{12}C \rightarrow {}^{7}Be$	1.54 ±3	30.8 ±6
$BeO \rightarrow {}^{7}Be$	Average		31.2 ±6
$^{9}Be \rightarrow {}^{7}Be$	$^{12}C \rightarrow {}^{11}C$	0.262 ± 4	12.8 ±5
$^{9}Be \rightarrow {}^{7}Be$	$^{27}Al \rightarrow {}^{18}F$	1.007 ± 4	12.6 ±6
$^{9}Be \rightarrow {}^{7}Be$	$^{12}C \rightarrow {}^{7}Be$	0.628 ± 2	12.6 ±6
$^{9}Be \rightarrow {}^{7}Be$	Average		12.6 ±6
$^{16}O \rightarrow {}^{7}Be$	$^{12}C \rightarrow {}^{11}C$	0.369 ± 6	18.0 ±7
$^{16}O \rightarrow {}^{7}Be$	$^{27}Al \rightarrow {}^{18}F$	1.56 ±7	19.5 ±8
$^{16}O \rightarrow {}^{7}Be$	$^{12}C \rightarrow {}^{7}Be$	0.910 ± 6	18.3 ±8
$^{16}O \rightarrow {}^{7}Be$	Average		18.5 ±7

TABLE IV. α-particle and p cross sections and $\sum_p^\alpha$ at $E_p = E_\alpha/N$ (230 MeV/N) and at $E_p = E_\alpha$ (920 MeV). The α-particle cross sections are from this work except for $\sigma[^{12}C(\alpha,x)^{11}C]$ from Ref. 3. The $^{16}O+p$ cross sections are from Refs. 2 and 14. The $^{12}C+p$ and $^{27}Al+p$ cross sections are from Ref. 13.

Reaction	ΔA	σ_α (mb) 920 MeV	σ_p (mb) 230 MeV	$\sum_p^\alpha$ $E_p = E_\alpha/N$	σ_p (mb) 920 MeV	$\sum_p^\alpha$ $E_p = E_\alpha$
$^{9}Be \rightarrow {}^{7}Be$	2	12.6 ±0.8	11.4±0.5	1.11±0.09	13.8 ±1	0.91±0.09
$^{12}C \rightarrow {}^{11}C$	1	48.9 ±2	38 ±2	1.29±0.08	28 ±1.4	1.75±0.1
$^{12}C \rightarrow {}^{7}Be$	5	20.0 ±1	9.9±1	2.04±0.2	10.0 ±1	2.00±0.2
$^{16}O \rightarrow {}^{15}O$	1	46.4 ±3	34 ±4	1.37±0.2	29 ±3	1.61±0.2
$^{16}O \rightarrow {}^{13}N$	3	6.75±0.5	5.0±1.5	1.35±0.4	5.0 ±2	1.35±0.5
$^{16}O \rightarrow {}^{11}C$	5	18.5 ±0.9	10 ±2	1.85±0.4	10 ±1.5	1.85±0.3
$^{16}O \rightarrow {}^{7}Be$	9	18.5 ±1	5.9±1.5	3.1 ±0.8	8.0 ±1.5	2.31±0.5
					9.0 ±1.5 [a]	2.06±0.4
$^{27}Al \rightarrow {}^{18}F$	9	12.5 ±0.5	6.0±0.4	2.08±0.15	8.05±0.5	1.55±0.1

[a] At 2 GeV.

^{7}Be decaying targets attenuated the 511-keV annihilation γ ray and separated the β^+ active targets from the NaI by an additional 0.16 cm. To correct for the last effects, a ^{7}Be active target was counted inside the Cu plates in the β^+ counting configuration and on the NaI in the ^{7}Be counting configuration, and a comparison of the count rates between the two counting configurations yielded a correction of (14.5±2)% to the ^{7}Be counting efficiency from just the Cu plates.

The self-absorption of the targets was theoretically corrected assuming that each emitted γ ray, on the average, traverses half of the target thickness which has a mass absorption coefficient of 0.07 g^{-1} cm^2. The largest correction was (3 ±1)% for the 10.8-g BeO target and was neglegible for the other targets. The correction to an infinitely thin target was made with the assumption that the correction for all targets and all product nuclei was the same and equal to the $^{12}C(\alpha, \alpha n)^{11}C$ depth effect in polystyrene[3,4] of (0.26±0.16)%/100 mg cm^{-2}. The 0.16-cm polystyrene disks were assumed to lose (0.4±0.4)% of the ^{11}C by diffusion.[11,12]

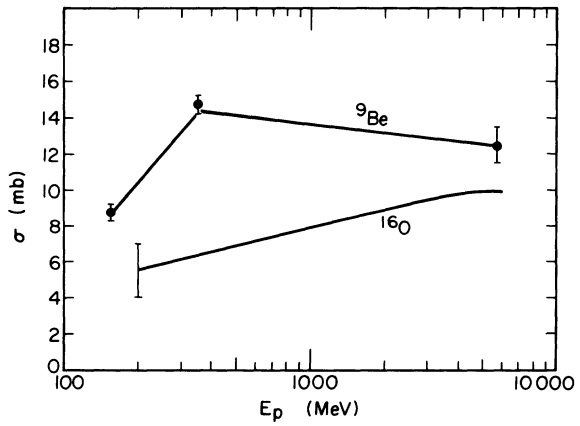

FIG. 2. ^{7}Be excitation functions for $p+{}^{9}Be$ and $p+{}^{16}O$ (from the references, see text). The error bar on the ^{16}O curve is constant for the length of the curve.

The random errors were: (1) Initial decay rate of the isotopes produced (Table II and text); (2) time at end of exposure (±1 sec); (3) background in the interval examined (81±1 counts/min); (4) target alignment (±1%); (5) diffusion loss of ^{11}C in the polystyrene (±0.4%); (6) uncertainty in the monitor cross sections (Table III).

The systematic errors are: (1) relative efficiency of the NaI(Tl) crystal for a 478-keV γ ray (±1%); (2) annihilation-γ sum peak (±0.2%); (3) annihilation-γ absorption in the target holder (±2%); (4) contamination in the BeO (±1%).

The random and systematic errors, where apropos, were separately rms combined and then added to give the error estimates in Tables II and III.

COMPARISON OF α AND p SPALLATION REACTIONS

In Table IV are tabulated the α-particle cross sections at $E_\alpha = 920$ MeV and the p cross sections at $E_p = E_\alpha$ and $E_p = E_\alpha/4$ (E_p equal to the same energy of a constituent nucleon of the α particle, i.e., $v_p = v_\alpha$). The $^{9}Be(p,x)^{7}Be$ cross sections at the two proton energies were taken from the excitation function (Fig. 2) which was determined from the adjusted cross sections listed in Table V. The adjusting factor for Parikh is the ratio of $\sigma[^{12}C(p,x)^{7}Be]$, measured by him (8.3±0.3 mb), to that of Cumming (10.2±1 mb).[13] The adjusting factor for Benioff is the ratio of $\sigma[^{27}Al(p,x)^{18}F]$, used as a monitor by him (7.68 mb), to that of Cumming (6.5±0.4 mb).[13]

The $^{16}O(p,x)^{7}Be$ excitation function, included in Fig. 2 for convenience, is derived from the

TABLE V. The ^{9}Be$(p,x)^7$Be cross section with adjustments described in the text.

Energy (MeV)	σ (mb)	σ adjusted (mb)	Author
156	8.8±0.5	8.8±0.5	Valentin *et al.* [a]
352	12.0±0.5	14.8±0.6	Parikh [b]
5700	15	12.5±1	Benioff [c]

[a] L. Valentin, G. Albouy, J. Cohen, and M. Gusakow, Phys. Lett. 7, 163 (1963).
[b] V. Parikh, Nucl. Phys. 18, 646 (1960).
[c] P. Benioff, Phys. Rev. 119, 316 (1960); Lawrence Radiation Laboratory Report No. UCRL-8780, 1959 (unpublished).

compilation by Silberberg[14] wherein $\sigma[^{16}O(p,x)^7Be]$ over the range 200 MeV $\leq E_p \leq$ 2 GeV is fitted to

$$\sigma = 3.25 \log_{10}[E_p(\text{MeV})] - 1.75 \pm 1.5 \text{ mb},$$

and over the range $E_p > 6$ GeV to $\sigma = 10 \pm 1.5$ mb (Fig. 2).

We now examine Σ_p^α as a function of ΔA at $E_\alpha = 920$ MeV. In Figs. 3 and 4 are plotted Σ_p^α vs ΔA (the net nucleon difference between target initial and final states), when constructed with $E_p = E_\alpha$ and $E_p = E_\alpha/4$, respectively. We notice in Figs. 3 and 4 that Σ_p^α for ^{12}C and ^{16}O targets for $\Delta A = 1$ (neutron) and $\Delta A = 5$ ($2p3n$ or any combination thereof) are less than one standard deviation from each other—a similarity suggesting similar nuclear structure for ^{12}C and ^{16}O. Further comparison between Figs. 3 and 4 shows a smoother variation of Σ_p^α when constructed with $E_p = E_\alpha$ (Fig. 3) than when constructed with $E_p = E_\alpha/4$ (Fig. 4). This observation is consistent with previous studies of $\Sigma_p^\alpha(^{12}C, ^{11}C)$[3,4,5] and of Σ_p^α in higher higher-Z targets.[15-17]

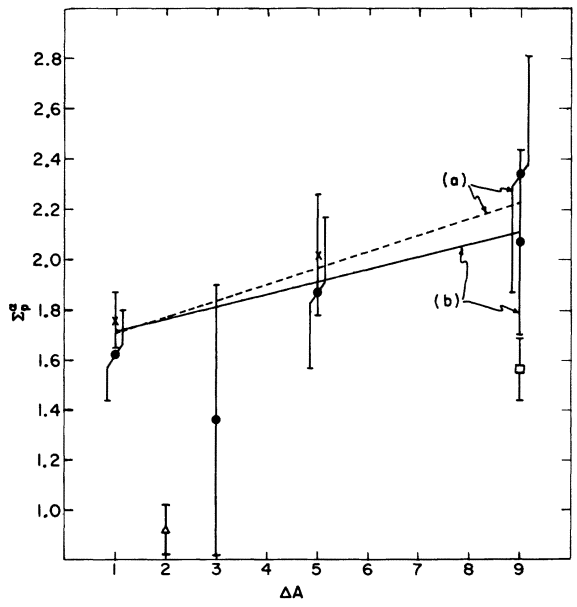

FIG. 3. Σ_p^α with $E_p = E_\alpha = 920$ MeV. □, ^{27}Al target; ●, ^{16}O target; ×, ^{12}C target; △, ^{9}Be target. Curves (a) and (b) are the linear fits of Σ_p^α (ΔA) to the ^{12}C and ^{16}O target cross sections, with the values for $\sigma[^{16}O(p,x)^7Be]$ at 2 GeV (a) or at 920 MeV (b).

In Fig. 3 are drawn the least-squares fits of $\Sigma_p^\alpha(\Delta A) = a + b\Delta A$ to the ^{12}C and ^{16}O spallation constructed with $E_p = E_\alpha$. The fit is sensitive to $\Sigma_p^\alpha(^{16}O, ^7Be)$. The values of $\sigma[^{16}O(p,x)^7Be]$ from Table IV at 1 GeV (or 2 GeV) of 8.0±1.5 mb (or 9.0±1.5 mb) yield $\Sigma_p^\alpha(^{16}O, ^7Be) = 2.31 \pm 0.5$ (or 2.06±0.4), and the coefficients in the $\Sigma_p^\alpha(\Delta A)$ linear fit of $a = 1.64 \pm 0.1$ (or 1.66±0.1) and $b = 0.062 \pm 0.04$ (or 0.048±0.04), and χ^2 per degree of freedom in both cases of 0.3. We conservatively chose the set of parameters inside the parenthesis for $\Sigma_p^\alpha(\Delta A)$ to scale all of the α-particle cross sections onto the p cross sections for the cosmic-ray transport calculation presented in the following section.

COSMIC-RAY PROPAGATION

The interactions of cosmic-ray nuclei ($\simeq$ 2 GeV/N) with the interstellar gas were parametrized by (1) the mean free path for absorption (Λ_{abs}), (2) the fragmentation probability of the absorbed i nucleus transmuting into the j nucleus (P_{ij}), and (3) the ionization-energy loss of the isotopes. We made the assumption that cosmic rays consist only of $L(Z = 3-5)$ and $M(Z = 6-9)$ isotopes and we investigated the sensitivity of the quantity $\Lambda(L/M = 0.25)$ and the abundances of the L and M elements to the He/H+He ratio of the interstellar gas. In addition, we examined the sensitivity of these two quantities to the separate variations of the three interaction parameters (Λ_{abs}, P_{ij}, and dE/dx) to gain a better understanding of the phenomena and to discern which parameters are most crucial, and consequently, which most need improved experimental accuracy. The one-dimensional transport equation used (a variation of that used by Appa Rao and Kaplon[18,19]), iterated in steps of $\Delta x = 0.1$ g/cm^2, is

$$N_i'(E_i, x+\Delta x)dE_i = N_i(E_i, x)e^{-\Delta x/\Lambda_i}dE_i + \sum_{j>i} N_j'(E_j, x+\Delta x) \times P_{ji}(1 - e^{-\Delta x/\Lambda_j})dE_j, \quad (1)$$

where the following definitions and formulas are used: all energies are in kinetic energy/nucleon; $N_i(E_i, x)dE_i$ is the flux of isotope i from E_i to $E_i + dE_i$ after traversal of x g/cm^2, the prime indi-

cates that the functional form of $N_i(E, x)$ is altered in transmission through Δx g/cm^2; F_i is the fraction of atoms of interstellar gas of element i (H and He), e.g., $F_{He} = He/H + He$; m_i is the mass of element i in grams; $\sigma^{re}_{i,k}$ is the reaction cross section for isotope i in target k ($k = p, \alpha$); $\sigma^{i}_{j,k}$ is the cross section for production of i from $j + k \rightarrow i + ,$ ($k = p, \alpha$); Λ_j is the mean free path for interaction in g/cm$^2 = \sum_{k=p}^{\alpha} F_k m_k / \sum_{i=p}^{\alpha} F_i \sigma^{re}_{j,i}$; and P_{ji} is the fragmentation probability $\sum_{l=p}^{\alpha} F_l \sigma^{i}_{j,l} / \sum_{k=p}^{\alpha} F_k \sigma^{re}_{j,k}$.

11 isotopes are transported—^{6}Li, ^{7}Be, ^{7}Li, ^{9}Be, ^{10}B, ^{11}B, ^{12}C, ^{13}C, ^{14}N, ^{15}N, and ^{16}O. ^{7}Be is considered stable. For simplicity ^{10}Be, whose p-spallation production cross section[20] in ^{16}O is < 0.1 that of ^{7}Be, is neglected (although results by Fontes *et al.*[5] for $p + {}^{12}$C spallation at 600 MeV show the ^{10}Be/^{7}Be ratio to be 0.25 ± 0.03, indicating that the ^{10}Be is nonnegligible). The calculation is performed at 2 GeV/N. The source spectrum is taken to be rigidity-dependent with spectral index -2.2.[21] This number is less than the usual rigidity spectral index of -2.6; however, at 2 GeV/N the calculation is insensitive to this parameter as all isotopes are minimum ionizing. The source distribution is taken to be 0.0 except for $^{12}C : {}^{14}N : {}^{16}O = 1.00 : 0.11 : 1.06$ (Ref. 22). The proton cross sections are taken from Beck and Yiou[23] and Yiou, Seide, and Bernas.[20] The cross sections used here differ from those of Beck and Yiou only for the ^{6}Li, ^{7}Li, ^{9}Be, and ^{10}B production cross sections in ^{16}O, taken here as 13.5, 13.5, 3.3, and 14 mb, respectively. The α-particle cross sections are treated as follows.

We seek to extrapolate our measurements of α-spallation cross sections at 920 MeV to the energy region of 8 GeV (2 GeV/N). In previous work it was shown that $\Sigma^{\alpha}_{p}(^{12}C, {}^{11}C)$, when constructed with $E_p = E_\alpha$, is constant ($= 1.7$) over the energy interval 380–920 MeV,[3,4] dipping slightly to a value of 1.4[4,5] when extending to the energy $E_\alpha = 150$ MeV. Over the same energy interval the ratio $\Sigma^{\alpha}_{p}(^{12}C, {}^{11}C)$, when constructed with $E_p = E_\alpha/4$, varies.[3,4] It is empirically observed that spallation cross sections in the light elements are nearly constant above 1 GeV[2]; in particular, the well measured $^{12}C(p, pn)\,^{11}C$ cross section is constant within experimental errors ($\pm 5\%$) from 1 to 30 GeV.[13] It appears safe to assume that $\Sigma^{\alpha}_{p}(^{12}C, {}^{11}C)$, when constructed with $E_p = E_\alpha$, remains constant when we extend the energy range from 920 MeV to 10 GeV; and it is probably safe to extend this argument to all "simple" reactions (0–2 nucleons removed), i.e., that $\Sigma^{\alpha}_{p}(\Delta A = 0\text{–}2)$, when constructed with $E_p = E_\alpha$, is constant in the energy region 1–10 GeV. In addition, for the purposes of the cosmic-ray transport calculation at 2 GeV/N, we make the ansatz that Σ^{α}_{p}, when constructed with $E_p = E_\alpha$, for each initial- and final-state nuclide belonging to the L and M groups, is constant in the energy range 1–10 GeV. As proton-spallation cross sections vary little from 1–10 GeV, [2] we deduce that the α-particle spallation cross sections, which we measured at 920 MeV, will have the same values at 8 GeV (2 GeV/N). In our transport calculation we use $\Sigma^{\alpha}_{p}(\Delta A) = a + b\Delta A$ with $a = 1.66 \pm 0.1$ and $b = 0.048 \pm 0.04$, which we derived earlier for reactions at $E_\alpha = 920$ MeV, to scale all of the α-particle cross sections onto the p cross sections using the proton-spallation cross sections at $E_p = 2$ GeV.

The spallation process in the Serber two-step model[24] is considered as a knock-on plus evaporation. Munir has shown[25] that the L nuclei produced in $p + M$ nuclei reactions at $E_p = 1$ GeV can be interpreted as evaporation residues with, on the average, small ($\approx$ 12-MeV) energy transfers. For all spallation reactions we have taken the initial and final kinetic energy per nucleon to be equal.

Values for $\Lambda_{^4He\ abs}$ had to be derived from models as, to the authors' knowledge, there have been no experiments measuring inelastic or absorption cross sections of ^{4}He nuclei of known energy (>100

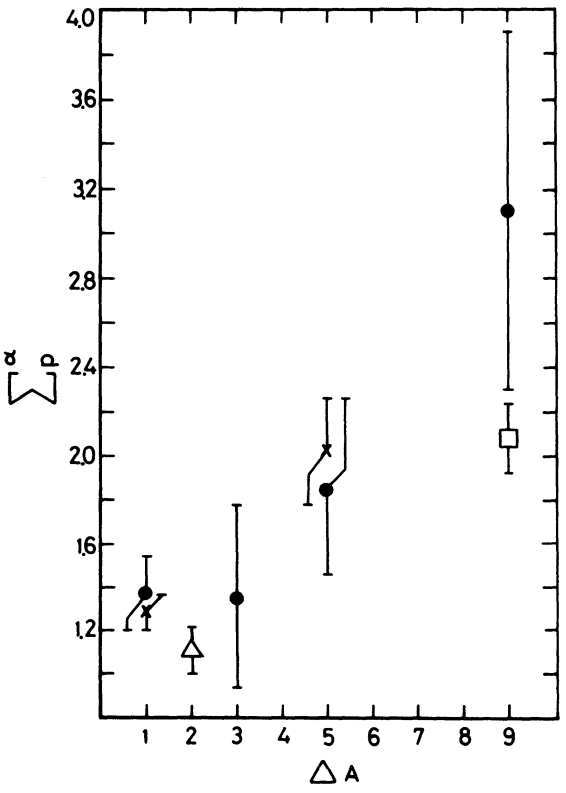

FIG. 4. Σ^{α}_{p} with $E_p = E_\alpha/N = 230$ MeV/N. □, ^{27}Al target; ●, ^{16}O target; ×, ^{12}C target; △, ^{9}Be target.

TABLE VI. Intercomparison of different models for interaction mean free paths in emulsion and air.

	Adopted experimental value	Independent-particle optical potential [a]	Three overlap models $\sigma^{re}_{i,\alpha}=\pi(r_0A_\alpha^{1/3}+r_0A_i^{1/3}-\Delta r)^2$		
r_0 (fm)			1.45 [b]	1.17 [c]	1.20 [d]
Δr (fm)			1.70 [b]	0.0 [c]	0.50 [d]
Λ_{emul} (g/cm^2) [e]	77 [f]	75.6 ± 0.3 [g]	77.6	69.9	77.9
Λ_{air} (g/cm^2)	44 [f]	42.5	47.0	36.2	42.9
$\sigma^{re}_{^{16}O,\alpha}$ (mb)		600 ± 10 [h]	569	725	616

[a] With a free nucleon-nucleon cross section of 40 mb. See Ref. 27.
[b] See Ref. 28.
[c] See Ref. 29.
[d] See Ref. 30.
[e] With $\sigma^{re}_{\alpha,p}=125$ mb. See Ref. 35.
[f] See text.
[g] Value read from a graph in Ref. 27 and adjusted with $\sigma^{re}_{\alpha,p}=125$ mb.
[h] Value read from a graph in Ref. 27.

MeV/N) in single-element targets [there are recent $(\alpha, \alpha n)$ cross-section measurements in $Z \geq 28$ targets by Church[26]]. We compared two nucleus-nucleus reaction cross-section models; (a) the independent-particle optical-potential model of Alexander and Yekutieli[27] (with a free nucleon-nucleon cross section of 40 mb), and (b) three versions of the overlap model

$$\sigma^{re}_{i,\alpha}=\pi(r_0A_\alpha^{1/3}+r_0A_i^{1/3}-\Delta r)^2 \quad (2)$$

first proposed by Bradt and Peters ($r_0=1.45$ fm, $\Delta r=1.70$ fm)[28] and modified by Daniel and Durgaprasad ($r_0=1.17$ fm, $\Delta r=0$)[29] and by Cleghorn, Freier, and Waddington ($r_0=1.20$ fm, $\Delta r=0.50$ fm).[30] Tests of the models come from the many experiments measuring $\Lambda_{\text{He abs}}$ of cosmic-ray α particles in emulsion (e.g., compilation by Waddington[31]) and the attenuation mean free path (Λ_{atn}) of cosmic-ray α-particles in the atmosphere. From the measurements of the latter quantity by Webber and McDonald,[32] Davis, Caulk, and Johnson,[33] McDonald,[34] and Webber and Ormes[21] of 43 ± 8, 35 ± 7, 45 ± 7, and 52 ± 4 g/cm^2, respectively, the value of 44 g/cm^2 was chosen. In calculating $\Lambda_{4_{\text{He abs}}}$ in emulsion we used $\sigma^{re}_{\alpha,p}$ of 125 mb.[35] In identifying $\Lambda_{4_{\text{He abs}}}$ in L and M elements from emulsion experiments, there is uncertainty in that $\approx 60\%$ of the reactions occur with Ag and Br and $\approx 30\%$ with C, N, and O. In air there is uncertainty arising from the fragmentation of the heavier-than-He cosmic rays and from the $^4\text{He} \rightarrow {}^3\text{He}$ stripping reactions. In air, we have estimated the errors as a result of equating $\Lambda_{4_{\text{He abs}}}=\Lambda_{\text{He atn}}$ from the two above processes, to be $\approx(9-14)\%$ and $\leq 30\%$, respectively (see Appendix). Consequently, for air we have taken $\Lambda_{4_{\text{He abs}}}=\Lambda_{\text{He atn}}=44$ g/cm^2 and for emulsion we have taken $\Lambda_{4_{\text{He abs}}}=77$ g/cm^2. In Table VI the four models are intercompared. The overlap model of Cleghorn, Freier, and Waddington[30] was chosen, but tests of all the models showed that the choice was inconsequential; it yielded less than 0.5% differences in the quantity $\Lambda(L/M=0.25)$ when using He/H+He = 0.2.

In Table VII (and Figs. 5 and 6) are tabulated the results of the calculation. Columns 1–3 give the value of He/H+He used for the individual parameters Λ_i, P_{ij}, and dE/dx with which we characterized interactions with the interstellar gas; columns 4–7 are the quantity $\Lambda(L/M=0.25)$ in g/cm^2 and atoms/(cm$^2 N_0$). Columns 8–12 are the resulting elemental ratios with respect to carbon at $L/M=0.25$. In row 1 are the observed elemental ratios from the experiments of von Rosenvinge, Ormes, and Webber,[7] von Rosenvinge and Webber,[8] Lezniak *et al.*,[36] and from the compilations of Shapiro, Silberberg, and Tsao.[22,37] Row 2 gives the calculated elemental ratios for He/H+He = 0.0. For the remaining rows, the elemental ratios are in percent differences from the ratios calculated with He/H+He = 0.0. In rows 5–8 and 9–12 we separately varied the quantity He/H+He for the parameters Λ_i, P_{ij}, and dE/dx one at a time to gain a better understanding of the phenomena and to learn to which parameters the cosmic-ray abundance ratios are most sensitive. The cases of the separate variation with He/H+He = 0.1 were derived from the cases of the separate variation with He/H+He = 0.2 by multiplying by the factor 0.541 (see following paragraph). In Table VII (bottom row) we again set He/H+He = 0.2 for only P_{ij}, but here we scaled the α-particle cross sections onto the proton cross sections with a constant scaling factor $\Sigma_p^\alpha(\Delta A)=2.0$. Comparing this

last result with that obtained when again setting He/H + He = 0.2 for only P_{ij}, but scaling the α-particle cross sections in our usual way by $\Sigma_p^\alpha = 1.66 + 0.048\Delta A$ (Table VII, row 6), we observe in general, much smaller effects on the elemental ratios for the case of $\Sigma_p^\alpha = 2.0$. This situation is expected, for with this scaling the α particle behaves merely as a big proton. We recall that the parameters Λ_i and dE/dx are not affected by the choice of Σ_p^α.

The fractional changes $[F(R)]$ in the quantity $\Lambda(L/M = 0.25)$ and the elemental ratios for $R \equiv$ He/H + He = 0.1 and 0.2, relative to $R = 0.0$, were fitted to $F(R) = g\mathrm{Re}^{-hR}$ where g and h are free parameters. Normalizing on $F(0.1) = 0.1$ and allowing for a multiplicative constant (g) for each of the fitted quantities (Table VII, row 3, He/H + He = 0.1 for Λ_i, P_{ij}, and dE/dx), yields $h = 0.78 \pm 0.3$ and $F(0.1)/F(0.2) = 0.541 \pm 0.02$. The fractional increase in the quantity $\Lambda(L/M = 0.25)$ over the range $0 \leq$ (He/H + He) ≤ 1.0, fitted to the same functional form (unnormalized), produced $g = 1.94$ and $h = 0.560$ (Fig. 7). Differences between the fitted $[F(R)]$ and calculated values in this instance (Fig. 7) were <3%.

In Fig. 5 we present the results of the transport calculation tabulated in Table VII. Under the heading of each element are four columns, three of which correspond to the separate variation, one at a time, of the He/H + He value used for the three interaction parameters Λ_i, P_{ij}, and dE/dx; and in the forth column is both the sum of the three previous columns and the results for the real case of the simultaneous variation of the He/H + He value used for Λ_i, P_{ij}, and dE/dx. In Fig. 6 is presented the quantity [(percent elemental-abundance change) − (average percent elemental-abundance change in L or M group)], which quantity is decoupled from the carbon variations found in the elemental ratios. We observe in both Figs. 5 and 6 that of the three interaction parameters Λ_i, P_{ij}, and dE/dx, that the elemental abundances are most sensitive to P_{ij} (Figs. 5 and 6, column 2 of each element). As we noted earlier, this effect arises from the nonzero slope of $\Sigma_p^\alpha(\Delta A)$ used in scaling the α-particle cross sections onto the proton cross sections. Although the quantity $\Lambda(L/M = 0.25)$ in terms of g/cm^2 and atoms/cm^2 N_0 are altered by + 19 and − 8%, respectively, by the inclusion of a 10% admixture of helium to the interstellar gas (Table VII), we observe in Table VII and Figs. 5 and 6 that the alterations of the elemental-abundance ratios to carbon are small (< 2%). A more detailed analysis is found in Ref. 4.

Until a few years ago, the slab approximation to the transport problem, i.e., a δ function path-length distribution,[38] had been the accepted model.

TABLE VII. Quantity of interstellar gas traversed and elemental ratios to carbon, parametrized by the He/H + He ratio of the interstellar gas at $L/M = 0.25$. Uncertainties on the signed (+ or −) fractional-elemental ratio changes arising from computer-printout "round off" are ≤5%.

Value of He/H + He used for			Amount of gas traversed				Elemental ratios to carbon [a]				
Λ_i	P_{ij}	dE/dx	g/cm^2	% [b]	atoms/cm^2 N_0	% [b]	Li	Be	B	N	O
Experimental observations [c]							0.15 ± 0.01	0.12 ± 0.02	0.27 ± 0.02	0.26 ± 0.02	0.89 ± 0.02
0.0	0.0	0.0	4.61	···	4.61	···	0.15	0.083	0.29	0.26	0.83
0.1	0.1	0.1	5.49	+19.2	4.23	−8.16	+1.47	+1.00	−0.62	−0.53	+0.77
0.2	0.2	0.2	6.24	+35.5	3.91	−15.1	+2.81	+1.85	−1.14	−0.95	+1.43
0.2	0.0	0.0	5.67	+23.0			+0.40	+0.65	+1.31	+0.27	+2.30
0.0	0.2	0.0	5.04	+9.49			+2.21	+0.76	−2.90	−2.01	−1.50
0.0	0.0	0.2	4.62	+0.33			+0.13	+0.27	+0.17	+0.42	+0.35
Sum of the partial He/H + He = 0.2				+32.8			+2.74	+1.68	−1.42	−1.32	+1.15
0.1	0.0	0.0	5.18	+12.4			+0.22	+0.35	+0.71	+0.15	+1.24
0.0	0.1	0.0	4.84	+5.13			+1.20	+0.41	−1.57	−1.09	−0.81
0.0	0.0	0.1	4.62	+0.19			+0.07	+0.15	+0.09	+0.23	+0.19
Sum of the partial He/H + He = 0.1				+17.7			+1.49	+0.91	−0.77	−0.71	+0.62
0.0	0.2 [d]	0.0	4.94	+7.2			+0.27	−0.34	−0.11	+0.11	−1.40

[a] Except for rows 1 and 2, the same as in footnote b; row 2 is the calculated values.
[b] Percent difference from the case of interstellar gas consisting of 100% hydrogen (row 2).
[c] See Refs. 7, 8, 22, 36, and 37.
[d] With $\sum_p^\alpha = 2.0$.

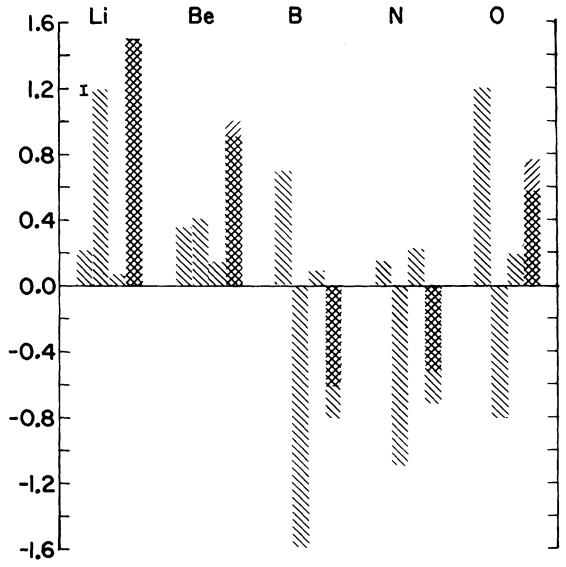

FIG. 5. Percent change in the cosmic-ray elemental-abundance ratios (to carbon) for He/H+He=0.1 from their values when He/H+He=0.0 at $L/M=0.25$. Under the heading of each element are four columns. The first three columns correspond to the separate variation, one at a time, of the He/H+He value used for the three interaction parameters. The parameter of interaction for which He/H+He=0.1 are: column 1, (Λ); 2, (P_{ij}); 3, (dE/dx). Column 4 contains both the sum of columns 1–3, \\\\, and the real case of the simultaneous variation of the He/H+He value used for Λ, P_{ij}, and dE/dx, ////. The error flag estimates the uncertainty from computer printout "round off".

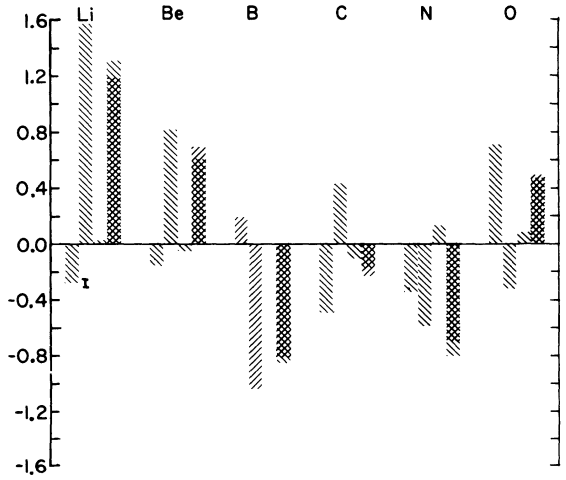

FIG. 6. The quantity [(percent change in elemental abundance) – (average percent change in elemental abundance in L or M group)] for He/H+He=0.1 compared to He/H+He=0.0. See caption of Fig. 5 for an explanation of subtitles.

A more theoretically satisfying model, which also produced better agreement with experiments, is the exponential path-length model.[38,39] The path-length model chosen is a second-order effect on changes in the abundances of the cosmic-ray L and M elements due to variation of the interstellar He/H+He ratio. Examining the fractional changes in the quantity $[L/M(\mathrm{He/H+He}=0.2)-L/M(0.0)]/[L/M(0.0)]$ between its value at $x=0.5$ g/cm^2 and its value at $x=5.0$ g/cm^2 of interstellar gas transversed, we concluded that differences arising in all the calculated fractional changes in the quantities of Table VII between the slab and exponential path-length models are < 5%.

CONCLUSIONS

The α-particle cross sections in ^{12}C and ^{16}O appear to scale onto the corresponding p cross sections when comparison is made on the basis of $E_p=E_\alpha$. A slow variation in the scaling factor Σ_p^α as a function of ΔA is observed. In incorporating the α-spallation cross sections into the cosmic-ray transport calculation we find that the $\approx 10\%$ component of the interstellar gas does not have pronounced effects (<2%) on the elemental abundances of the cosmic-ray L and M groups at 2 GeV/N. As a consequence of the nonconstant $\Sigma_p^\alpha(\Delta A)$, the P_{ij}, in general have a greater effect on the elemental ratios than does Λ_i. It is to be noted that $\Sigma_p^\alpha(^{16}\mathrm{O}, ^7\mathrm{Be})$, when constructed with $E_p=E_\alpha/N=230$ MeV/N, is 3.1 ± 0.8 owing to the lower value of $\sigma[^{16}\mathrm{O}(p,x)^7\mathrm{Be}]=5.9\pm1.5$ mb (see text, Fig. 2, and Ref. 14) at this energy. The $\approx 10\%$ He in the interstellar gas at this energy is responsible for $\approx 20\%$ of the ^{7}Be production. To further investigate the role of interstellar helium in cosmic-

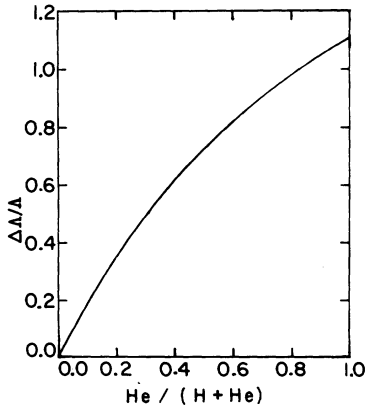

FIG. 7. Fractional change in the quantity $\Lambda(L/M=0.25)$ as a function of $R\equiv$ He/H+He. The curve is a fit to $\Delta\Lambda/\Lambda=1.94R\exp(-0.56R)$ which differs from the calculated fractional change by < 3% for all R.

ray interactions, additional data are needed for the α-spallation reactions in Fe L and M groups at $E_\alpha > 50$ MeV/N.

ACKNOWLEDGMENTS

We thank the members of the Cosmic Ray Group at New York University for their support, advice, and discussion; in particular Serge A. Korff and Rosalind B. Mendell. We warmly thank and acknowledge the support and continuous aid of the Nuclear Emulsion Group at LBL, especially Harry H. Heckman, Douglass Greiner, and Peter Lindstrom. We thank Robert Kuntz of Lawrence Livermore Laboratory for providing the Be target. We are indebted to the 184-in. cyclotron crew headed by Jimmy Vale.

APPENDIX

^{4}He absorption in the atmosphere is usually estimated from the cosmic-ray helium flux which is measured by a particle detector attached to an ascending and/or descending balloon, and is a function of detector depth in the atmosphere. What is measured is the He attenuation mean free path ($\Lambda_{\text{He atn}}$) which is affected by the fragmentation of the $Z>2$ cosmic rays and by ^{4}He $\rightarrow$ ^{3}He stripping reactions (assuming that the detectors are unable to separate ^{4}He from ^{3}He). Using the transport equation [Eq. (1)] we can estimate the effect of the ^{4}He production from the fragmentation of the $Z>2$ cosmic rays. Neglecting ionization energy loss and reducing the incremental in x to a differential, we are left with (for He development)

$$\frac{d}{dx}\mathrm{He}(x)+\frac{1}{\Lambda_{\mathrm{He}}}\mathrm{He}(x)=\sum_{i\,(Z>2)}\frac{N_i(x)}{\Lambda_i}P_{i\mathrm{He}}. \qquad (3)$$

The equation for $N_i(x)$ is the same as the above for He, except for leaving off the source on the right-hand side (rhs). This introduces an error of significance only in the L group. $N_i(x)$ can then be written as $N_i(x)=A_i e^{-x/\Lambda_i}$, where A_i is the relative abundance to He at the top of the atmosphere. The rhs of Eq. (3) is 15% of the second term on the left-hand side at $x=0$ and diminishes as x increases ($\Lambda_i<\Lambda_{\mathrm{He}}$). The He functional form does not differ much from a simple exponential. Setting $\mathrm{He}(x)=e^{-x/\Lambda}$, and averaging the He flux over the first ζ g/cm^2 of the atmosphere [integrating Eq. (3) from $x=0$ to $x=\zeta$], we find

$$\frac{\Lambda-\Lambda_{\mathrm{He}}}{\Lambda}(1-e^{-\zeta/\Lambda})-\sum_{i\,(Z>2)}A_iP_{i\mathrm{He}}(1-e^{-\zeta/\Lambda_i})=0. \qquad (4)$$

Consistent with the approximation needs, we group the source elements into L, M, and H ($Z\geq 10$) groups. Using the fluxes of von Rosenvinge, Ormes, and Webber[7,8] and Webber and Ormes,[21] the ionization corrected Λ_{atn} of Webber and Ormes,[21] the $P_{i\mathrm{He}}$ in air of Friedlander *et al.*,[40] and Λ_{He} from Table V of 44 g/cm^2, we solve Eq. (4) for Λ, parameterized by ζ, and find:

ζ(g/cm^2)	20	50	100	150
Λ(g/cm^3)	50	49	48	48

These values of Λ are what one expects to measure in the atmosphere for $\Lambda_{\mathrm{He\,atn}}$ as a consequence of the spallation of the **heavier**-than-helium cosmic rays when given a true $\Lambda_{\mathrm{He\,abs}}$ of 44 g/cm^2. Thus equating in the atmosphere $\Lambda_{\mathrm{He\,abs}}$ to $\Lambda_{\mathrm{He\,atn}}$ may introduce an overestimation of $\Lambda_{\mathrm{He\,abs}}$ of $\approx$ (9–14)%.

The effect on $\Lambda_{\mathrm{He\,abs}}$ measurements from ^{4}He $\rightarrow$ ^{3}He stripping in the atmosphere can be estimated from the $^4\mathrm{He}(n,np)^3\mathrm{H}$, $^4\mathrm{He}(n,d)^3\mathrm{H}$, and $^4\mathrm{He}(n,2n)^3\mathrm{He}$ cross sections of (55 ± 5), (2 ± 1), and (3 ± 1)% of $\sigma^{re}_{^4\mathrm{He},n}$, respectively, measured by Innes[41] at 300 MeV. If we invoke charge symmetry, the first two fractional cross sections should be equal to $\sigma[^4\mathrm{He}(p,pn)^3\mathrm{He}]/\sigma^{re}_{^4\mathrm{He},p}$ and $\sigma[^4\mathrm{He}(p,d)^3\mathrm{He}]/\sigma^{re}_{^4\mathrm{He},p}$. Averaging ^{3}He production over p and n targets

$$\frac{\sigma[^4\mathrm{He}(n,2n)^3\mathrm{He}]+\sigma[^4\mathrm{He}(p,pn)^3\mathrm{He}]+\sigma[^4\mathrm{He}(p,d)^3\mathrm{He}]}{2\sigma^{re}_{^4\mathrm{He},p}}=0.30\pm0.03 \qquad (5)$$

and assuming that this ratio holds in the atmosphere for $\sigma[^4\mathrm{He}(\mathrm{atm},\,)^3\mathrm{He}]/\sigma^{re}_{^4\mathrm{He},p}$, we have $\Lambda_{^4\mathrm{He\,abs}}=(1-P_{^4\mathrm{He},^3\mathrm{He}})\Lambda_{\mathrm{He\,abs}}=(1-0.30\pm0.03)\Lambda_{\mathrm{He\,abs}}=(0.70\pm0.03)\Lambda_{\mathrm{He\,abs}}$. The factor 0.70 ± 0.03 should be taken as a lower bound, as it is expected that the collisions of ^{4}He with the centers of ^{14}N and ^{16}O will be less effective than with the surfaces of ^{14}N and ^{16}O for single-nucleon knockouts from the ^{4}He. Thus, by equating in the atmosphere, $\Lambda_{\mathrm{He\,abs}}$ to $\Lambda_{^4\mathrm{He\,abs}}$, we overestimate $\Lambda_{^4\mathrm{He\,abs}}$ by $\lesssim 30\%$; viz., taking $\Lambda_{\mathrm{He\,abs}}=44$ g/cm^2, then $\Lambda_{^4\mathrm{He\,abs}}$, considering just stripping reactions, equals 31 g/cm^2—a small number in view of geometric calculations (Table VI).

*Work supported in part by the National Aeronautics and Space Administration under Grants Nos. NGL-33-016-067 and NAS1-5209, and by the U. S. Atomic Energy Commission.

†Work performed in part while at New York University, Department of Physics, New York City, N. Y. 10003.

[1]I. J. Danzinger, Ann. Rev. Astron. Astrophys. 8, (1970).

[2]J. Audouze, M. Epherre, and H. Reeves, in *High Energy Nuclear Interactions in Astrophysics*, edited by B. S. P. Shen (Benjamin, New York, 1967).

[3]J. Radin, Phys. Rev. C 2, 793 (1970); C 4, 1010 (1971).

[4]J. Radin, Ph.D. thesis, New York University, 1971 (unpublished). The present work is extracted from this thesis.

[5]P. Fontes, C. Perron, J. Lestringuez, F. Yiou, and R. Bernas, Nucl. Phys. A165, 405 (1971).

[6]J. Lestringuez, G. M. Raisbeck, F. Yiou, and R. Bernas, Phys. Lett. 36B, 331 (1971).

[7]T. T. von Rosenvinge, J. F. Ormes, and W. R. Webber, Astrophys. Space Sci. 3, 80 (1969).

[8]T. T. von Rosenvinge and W. R. Webber, Astrophys. Space Sci. 3, 4 (1969).

[9]C. M. Lederer, J. M. Hollander, and I. Perlman, *Table of Isotopes* (Wiley, New York, 1967), 6th ed.

[10]W. S. Gilbert, D. Keefe, J. B. McCaslin, H. W. Patterson, A. R. Smith, L. D. Stephens, K. B. Shaw, G. R. Stevenson, R. H. Thomas, R. D. Fortune, and K. Goebel, Lawrence Radiation Laboratory Report No. UCRL-17941, 1968 (unpublished).

[11]H. Fuch and K. H. Lindenberger, Nucl. Instrum. Methods 7, 219 (1960).

[12]J. B. Cumming, A. M. Poskanzer, and J. Hudis, Phys. Rev. Lett. 6, 484 (1961).

[13]J. B. Cumming, Annu. Rev. Nucl. Sci. 13, (1963).

[14]R. Silberberg, private communication; R. L. Silberberg and C. H. Tsao, Astrophys. J. Suppl. Ser. 220, 25, 315 (1973); see also Ref. 2.

[15]R. G. Korteling and E. K. Hyde, Phys. Rev. 136, B425 (1964).

[16]V. P. Crespo, J. M. Alexander, and E. K. Hyde, Phys. Rev. 131, 1765 (1963).

[17]L. Winsberg, Phys. Rev. 135, B1105 (1964).

[18]M. V. K. Appa Rao and M. F. Kaplon, Nuovo Cimento 27, 700 (1963).

[19]M. V. K. Appa Rao, Nuovo Cimento 32, 2582 (1964).

[20]F. Yiou, C. Seide, and R. Bernas, J. Geophys. Res. 74, 2447 (1969).

[21]W. R. Webber and J. F. Ormes, J. Geophys. Res. 72, 5957 (1967).

[22]M. M. Shapiro, R. Silberberg, and C. H. Tsao, Source Distribution of Cosmic Ray Abundances, presented at the Midwest Cosmic Ray Conference, Baton Rouge, Louisiana, 1969 (unpublished).

[23]F. Beck and F. Yiou, Astrophys. Lett. 1, 75 (1968).

[24]R. Serber, Phys. Rev. 72, 1114 (1947).

[25]B. A. Munir, Philos. Mag. 1 (Ser. 8), 355 (1956).

[26]L. B. Church, Phys. Rev. C 6, 1293 (1972).

[27]G. Alexander and G. Yekutieli, Nuovo Cimento 19, 103 (1961).

[28]H. L. Bradt and B. Peters, Phys. Rev. 77, 54 (1950).

[29]R. R. Daniel and N. Durgaprasad, Nuovo Cimento Suppl. 23, 82 (1962).

[30]T. F. Cleghorn, P. S. Freier, and C. J. Waddington, Can. J. Phys. 46, S572 (1968).

[31]C. J. Waddington, Prog. Nucl. Phys. 8, 1(1963).

[32]W. R. Webber and F. B. McDonald, Phys. Rev. 100, 1460 (1955).

[33]L. R. Davis, H. M. Caulk, and C. Y. Johnson, Phys. Rev. 101, 800 (1956).

[34]F. B. McDonald, Phys. Rev. 104, 1723 (1956).

[35]M. S. Kozodaev, M. M. Kulyukin, R. M. Sulyaev, A. I. Filippov, and Y. A. Scherbakov, Zh. Eksp. Teor. Fiz. 38, 708 (1960) [transl.: Sov. Phys.—JETP 38, 511 (1960)].

[36]J. A. Lezniak, J. F. Ormes, T. T. von Rosenvinge, and W. R. Webber, Astrophys. Space Sci. 5, 103 (1969).

[37]M. M. Shapiro and R. Silberberg, Acta Phys. 29, S485 (1970).

[38]M. M. Shapiro, R. Silberberg, and C. H. Tsao, Acta Phys. 29, S471 (1970).

[39]R. Cowsik, Y. Pal, S. N. Tandon, and R. P. Verma, Can. J. Phys. 46, S646 (1968).

[40]M. W. Friedlander, K. A. Neelakantan, S. Tokunaga, G. R. Stevenson, and C. J. Waddington, Phil. Mag. 8, 1691 (1963).

[41]W. H. Innes, University of California Radiation Laboratory Report No. UCRL-8040, 1957 (unpublished).